

# Rapid Softlithography Using 3D-Printed Molds

Sajad Razavi Bazaz, Navid Kashaninejad, Shohreh Azadi, Kamal Patel, Mohsen Asadnia, Dayong Jin, and Majid Ebrahimi Warkiani\*

Polydimethylsiloxane (PDMS) is a long-standing material of significant interest in microfluidics due to its unique features. As such, rapid prototyping of PDMS-based microchannels is of great interest. The most prevalent and conventional method for fabrication of PDMS-based microchips relies on soft-lithography, the main drawback of which is the preparation of a master mold, which is costly and time-consuming. To prevent the attachment of PDMS to the master mold, silanization is necessary, which can be detrimental for cellular studies. Additionally, using coating the mold with a cell-compatible surfactant adds extra preprocessing time. Recent advances in 3D printing have shown great promise in expediting microfabrication. Nevertheless, current 3D printing techniques are sub-optimal for PDMS softlithography. The feasibility of producing master molds suitable for rapid softlithography is demonstrated using a newly developed 3D-printing resin. Moreover, the utility of this technique is showcased for a number of widely used applications, such as concentration gradient generation, particle separation, cell culture (to show biocompatibility of the process), and fluid mixing. This can open new opportunities for biologists and scientists with minimum knowledge of microfabrication to build functional microfluidic devices for their basic and applied research.

## 1. Introduction

In recent years, there has been a new surge of interest in 3D printing, which is defined as building successive layers of materials to form a desired object.<sup>[1,2]</sup> The interest in 3D printing methods is twofold. First, the advent of 3D printing has triggered the creation of numerous intricate designs, whether in micro or macro scale, often implausible through conventional fabrication methods. Second, 3D printing enables quick evaluation

of ideated solutions, often within the same day. Feature-wise selection of printing parameters and multistep printing processes enable users to pay extra attention to the tiny details of their objects.<sup>[3]</sup> In addition, material specifications (e.g., Young modulus or transparency) can be adjusted based on the printing method. It is estimated that the market size of 3D printing will triple in the next half-decade, growing from 7.3 billion dollars in 2017 to 23 billion dollars by 2022.<sup>[4]</sup> As structures manufactured by 3D printing methods can be in the range of micrometers to centimeters, a new challenge emerges for microfabrication.<sup>[5]</sup>

The miniaturization of high-cost, resource demanding, and time-consuming lab processes into a high-efficient, multifunctionalized, and integrated microchip has been considered as a revolution across many fields of science.<sup>[6]</sup> Microfluidics, the commercial name for this revolution, is ubiquitous in fluid mechanics, reagent

mixture, cell biology, particle and cell separation, metabolomics and proteomics, forensic, and genetic analysis.<sup>[7,8]</sup> Microfluidic devices enjoy the proficiency of low reagent consumption, parallelization, portability, integrated several biological assays, small footprint, accurate measurement, and live feedback.<sup>[9]</sup> Compared to macroscale fluid handling, microfluidics provides end-users with an economical and ready-to-use microchip with faster reaction time and prompt analysis.<sup>[10,11]</sup>


S. Razavi Bazaz, Dr. N. Kashaninejad, S. Azadi, Dr. M. Ebrahimi Warkiani  
School of Biomedical Engineering  
University of Technology Sydney  
Sydney, New South Wales 2007, Australia  
E-mail: majid.Warkiani@uts.edu.au

K. Patel  
Creative CADworks  
Toronto, Ontario M5C 2M6, Canada

Dr. M. Asadnia  
Department of Engineering  
Faculty of Science and Engineering  
Macquarie University  
Sydney, New South Wales 2109, Australia

Prof. D. Jin, Dr. M. Ebrahimi Warkiani  
Institute for Biomedical Materials and Devices  
Faculty of Science  
University of Technology Sydney  
NSW 2007, Australia

Prof. D. Jin  
ARC Research Hub for Integrated Device for End-user Analysis  
at Low-levels (IDEAL)  
Faculty of Science  
University of Technology Sydney  
New South Wales 2007, Australia  
Dr. M. Ebrahimi Warkiani  
Institute of Molecular Medicine  
Sechenov University  
Moscow 119991, Russia

 The ORCID identification number(s) for the author(s) of this article can be found under <https://doi.org/10.1002/admt.201900425>.

DOI: 10.1002/admt.201900425

There is a growing body of literature that recognizes the significance of lithography in the fabrication of PDMS-based microchannels. However, lithography is limited in its ability to fabricate nonstraight microchannels. For instance, for vascular behavior imitation, fabrication of 3D complex vessel branches is mandatory.<sup>[12]</sup> Moreover, there are major limitations in the fabrication of angular designs, such as a microchannel with a trapezoidal cross-section.<sup>[13]</sup> Furthermore, nonplanar structures as well as 2D and 3D nanolithography always introduce more complexity to the fabrication process.<sup>[14]</sup> In addition, advanced equipment and an adroit operator are essential for microfabrication processes, especially when the surface coating of the device is of interest.<sup>[15]</sup> For these reasons, research groups have tried to provide alternative methods for the fabrication of molds used in softlithography processes.<sup>[16]</sup> One such alternative is the use of 3D printing technology for the fabrication of softlithography molds. Among all 3D printing methods, stereolithography apparatus (SLA) and digital light processing (DLP) offer great advantages, making them ideal candidates for microfluidics and biomedical applications.<sup>[17]</sup> However, one of the limitations of 3D printed SLA/DLP master molds for softlithography is the requirement for tedious pretreatments prior to PDMS casting. The pretreatment of the resin is necessary to ensure the complete curing of the PDMS in contact with the resin. Otherwise, the surface of the PDMS replica in contact with the resin cannot be polymerized due to the presence of residual catalyst and monomers, and its transparency would be also compromised.<sup>[18]</sup> It has been observed that the effects of pretreating the master mold are more significant in channels with smaller feature sizes,<sup>[19]</sup> and, in the case of relatively larger 3D printed parts, this challenge is not significant.<sup>[20]</sup> To address this issue, many researchers have proposed various pretreatment protocols to treat the 3D printed master mold before PDMS casting.<sup>[18,19,21–24]</sup> As one of the first attempts, Comina et al. proposed to cover the 3D printed template with a specialized ink via airbrushing.<sup>[21]</sup> However, the effectiveness of that method depended largely on the thickness of the ink. Four procedures are commonly used among other proposed postprinted protocols: 1) UV curing; 2) surface cleaning (e.g., ethanol sonification and soaking); 3) preheating; 4) surface silanization. Waheed et al. introduced an efficient yet time-consuming pretreatment protocol for PDMS softlithography.<sup>[24]</sup> The post-processing included a 5 min UV treatment followed by 6 h of soaking in an ethanol bath. Following the air plasma treatment for 1 min, the surface of the 3D printed template was silanized by perfluorooctyl triethoxysilane for 3 h.

Nevertheless, there is still no consensus about the optimum protocol for treating 3D printed templates for PDMS casting. In addition, the proposed protocols are time-consuming, labor-intensive, and lacking reproducibility. Furthermore, the treatment parameters, such as UV curing time, preheating temperature, and duration, seem to be a function of the feature size; thus, differ from one experiment to another.<sup>[24]</sup> Also, preheating in particular is a common step in many procedures and often induces high levels of material strain, resulting in the formation of cracks within microstructures.<sup>[18,25]</sup> Most importantly, surface silanization of the 3D printed templates is essential to ensure the PDMS peels off, correctly. Some silanizing agents such as perfluorooctyl triethoxysilane are cytotoxic and are not

suitable for biological applications. Thus, development of a resin suitable for master mold fabrication will reduce all these time-consuming steps.

To address the aforementioned issues, herein, we optimize the use of a new resin developed by Creative CADworks (CCW Master Mold for PDMS devices) (i.e., made of methacrylated oligomers and monomers) for the fabrication of master molds directly by the DLP 3D printing method. We show that the 3D printed templates obtained using this resin can be immediately casted with PDMS without any pretreatment or surface modification. By way of explanation, the process of master mold design to microchip fabrication has been reduced from a time frame of several days (for a conventional softlithography process) to less than 5 h. In order to showcase the functionality of this resin, four different microfluidic devices have been developed. Each device represents a specific application, including separation, micromixing, concentration gradient generation, and cell culturing. The surface of the PDMS replica obtained from the 3D printed mold is also evaluated to investigate the bonding quality of PDMS.

## 2. Results and Discussions

### 2.1. PDMS Characterization

It is well-known that the quality of the PDMS casted on the mold can affect the whole performance of the microfluidic device.<sup>[26]</sup> Hence, its quality must be analyzed before use. After fabricating the 3D printed molds and removal of any residual resin, PDMS was casted on the master molds. For the sake of comparison, two different molds were fabricated, one with a conventional DLP resin and the other with the newly developed microfluidic resin. The main challenge with conventional DLP resin is that due to the presence of unreacted monomers, complete polymerization of PDMS cannot occur, resulting in the presence of residual material on both the PDMS and the mold, as shown in **Figure 1A**. The comparison between the mold fabricated via conventional resin and the microfluidic resin reveals that these two molds have identical surface roughness, and the smallest channel height for the fabrication of molds can be achieved with a thickness layer of 30  $\mu\text{m}$ . However, for this thickness layer, the curing time of each layer for the newly developed resin is 6.5 s, which is more than the conventional one which is 1.3–1.5 s; as more time must be devoted to the methacrylated resins to be completely polymerized and cured. All in all, the fabrication time for both molds took less than an hour which is much faster than other methods. Also, the inset in **Figure 2A** shows the contact angle of the 3D printed molds. The contact angle measurement reveals that both surfaces are hydrophilic; however, the microfluidic resin is slightly more hydrophilic than the conventional one.

By substituting the acrylate components with methacrylated monomers and oligomers (**Figure 1B**), we are able to create a clean temporary binding site between the PDMS and the 3D printed master mold. To demonstrate this, we applied both of the conventional DLP resin and the newly proposed microfluidic resin to a single design and investigated the bonding properties of PDMS. Both molds were subjected to the same

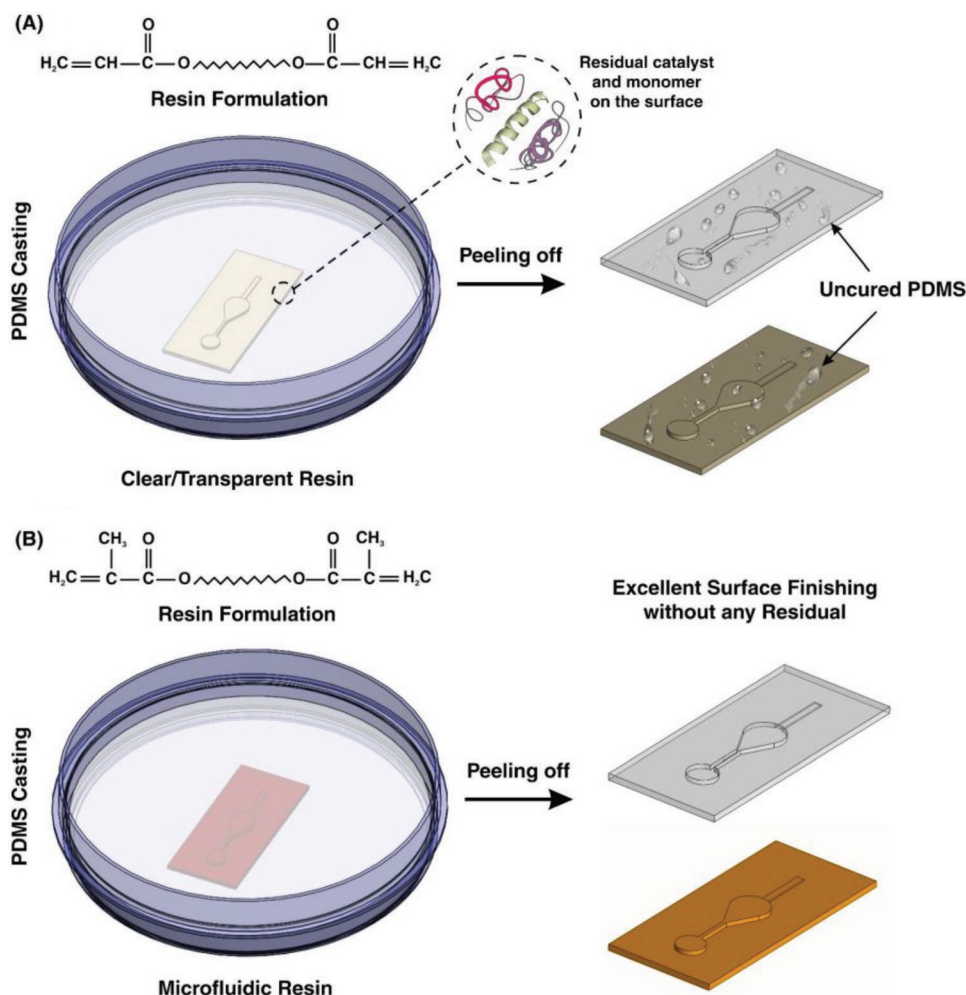


**Figure 1.** A) Schematic illustration of how acrylated DLP resins impact the surface finish of casted PDMS pieces. Residual catalysts and monomers present at the interface between the resin and PDMS impede the polymerization of PDMS components, leaving behind residual material. B) Demonstrating the improved performance of methacrylated resin over conventional acrylates in providing a smooth surface finish with no residual material. This is due to a lack of unreacted monomers and oligomers impeding the complete polymerization of PDMS.

experimental procedure. It has been proven that in UV-cured systems, cracks developed as a result of shrinkage forces between and after curing.<sup>[27,28]</sup> In the methacrylated systems, this shrinkage has an inverse relation to the initial viscosity.<sup>[28,29]</sup> As the modified resin is more viscous than the conventional ones, the chance of cracks appearing and propagating reduced significantly during the curing process. As such, the mold fabricated via the microfluidic resin has better stability and a very smooth surface compared to those fabricated by conventional resin. As Figure 2A indicates, in the conventional DLP resin, PDMS surfaces in contact with the surface of the resin were not properly cured, and uncured PDMS layers remained on both surfaces. It can be clearly seen that the casted PDMS fails to adopt the pattern of the mold, thoroughly. In addition, during the detachment of PDMS from the mold, PDMS tends to stick to the resin, confirming that the surface of the conventional DLP resin is not appropriate for PDMS casting. By analyzing the materials constituting the conventional DLP resin, it is believed that this problem is related to the chemical composition of the resin. We hypothesized that the remaining catalyst

and monomers on the surface of the printed mold disrupt the complete polymerization of a thin layer of PDMS in contact with the mold. This can be clearly seen upon the removal of the PDMS replica from the mold (Figure 2A). As such, the “acrylate group” in the resin’s chemistry is not a suitable choice for PDMS casting; this has urged different scientists to explore time-consuming strategies for the surface treatment of DLP printed molds. Through extensive research conducted by Creative CADworks, a new resin which contains methacrylated monomers and oligomers has been developed. Casted PDMS does not react with the methacrylated monomers because the surface of the mold is free of residual monomer units that may impede PDMS polymerization. As Figure 2B illustrates, once a blade cuts through the PDMS layer down to the mold, the PDMS replica detaches easily. The operation of each device and the quality of bonding were also analyzed for a wide range of flow rates (to check the simulations results of surface roughness and bonding quality, see Section 2.2) with the experimental setup shown in Figure 2C. The results, as shown in Figure 2D, confirmed that there was no leakage observed between flow



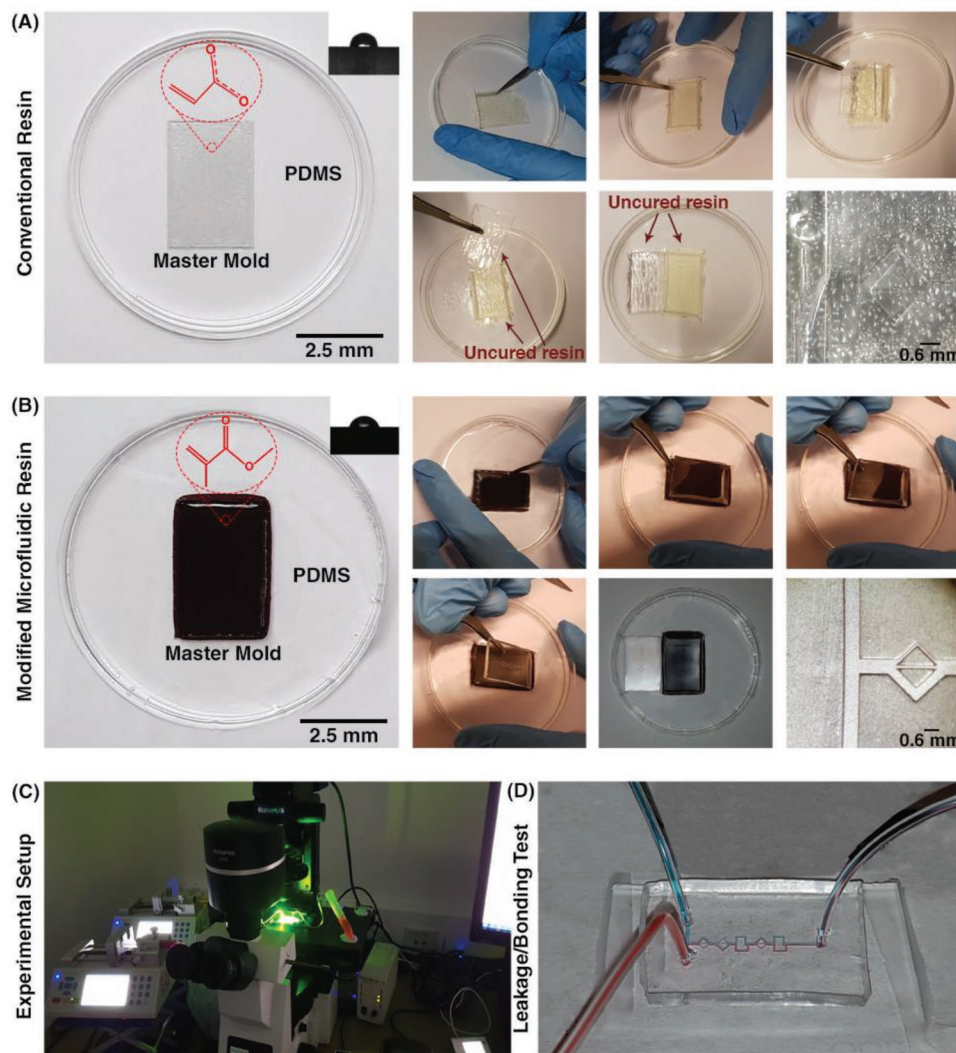


**Figure 2.** PDMS casting process in A) conventional DLP resin and B) microfluidic resin. The insets depict the contact angles on the surface of molds. In conventional resin, PDMS in touch with the surface of the mold cannot provide a temporary bonding, and the surface of the PDMS cannot replicate the pattern used in resin. In microfluidic resin, as soon as the blade reaches the surface of the mold, PDMS start to detach from the surface, and it can easily peel-off. The mold after PDMS casting in microfluidic resin clarifies that there is not any residual of PDMS on its surface, while in conventional DLP resin, residuals are on the surface. C) Experimental setup used in these series of experiments is illustrated. D) No leakage was seen during the experiments after bonding of PDMS by plasma surface treatment method.

rates ranging from 0.1 to 5 mL min<sup>-1</sup>, which indicates that the proposed method for fabricating PDMS-based microdevice is an ideal candidate for a variety of applications.

## 2.2. Simulation Studies of Surface Characterization

Here, the effects of surface roughness on the velocity and shear rate distribution along the length of microchannel were investigated through simulation study by COMSOL 5.3a. For a smooth surface,  $S_a$  was set as 0.3  $\mu\text{m}$ , and for a rough surface,  $S_a$  was assigned to be 1  $\mu\text{m}$ . Different flow rates of 0.1, 1, 1.7, and 3 mL min<sup>-1</sup> were tested to investigate the shear rates present in the devices. **Figure 3A** shows velocity and shear rate distribution along the length of the smooth microchannel

( $S_a = 0.3 \mu\text{m}$ ). The two insets (Figure 3AI, AII) depict shear rate distribution across the bottom surface of the microchannel at flow rates of 0.1 and 3 mL min<sup>-1</sup>; and by increasing the flow rate from 0.1 to 3 mL min<sup>-1</sup>, the order of the shear rate increased 100 times. Furthermore, the shear rate distribution illustrates that in the middle of the microchannel, due to the high shear rate, there is a higher probability for the quality of surface bonding to be disrupted than at the edge of the microchannel. Moreover, shear rate distribution 50  $\mu\text{m}$  from the inlet was investigated at heights of 2, 5, 10, and 15  $\mu\text{m}$  (half of the channel height) from the bottom surface for four flow rates of 0.1, 1, 1.7, and 3 mL min<sup>-1</sup> (Figure 3AIII–AVI). The trend observed illustrates that the shear rate is focused halfway across the width of the channel at the height of 2  $\mu\text{m}$ ; as the height increases, the focus is drawn away from the center

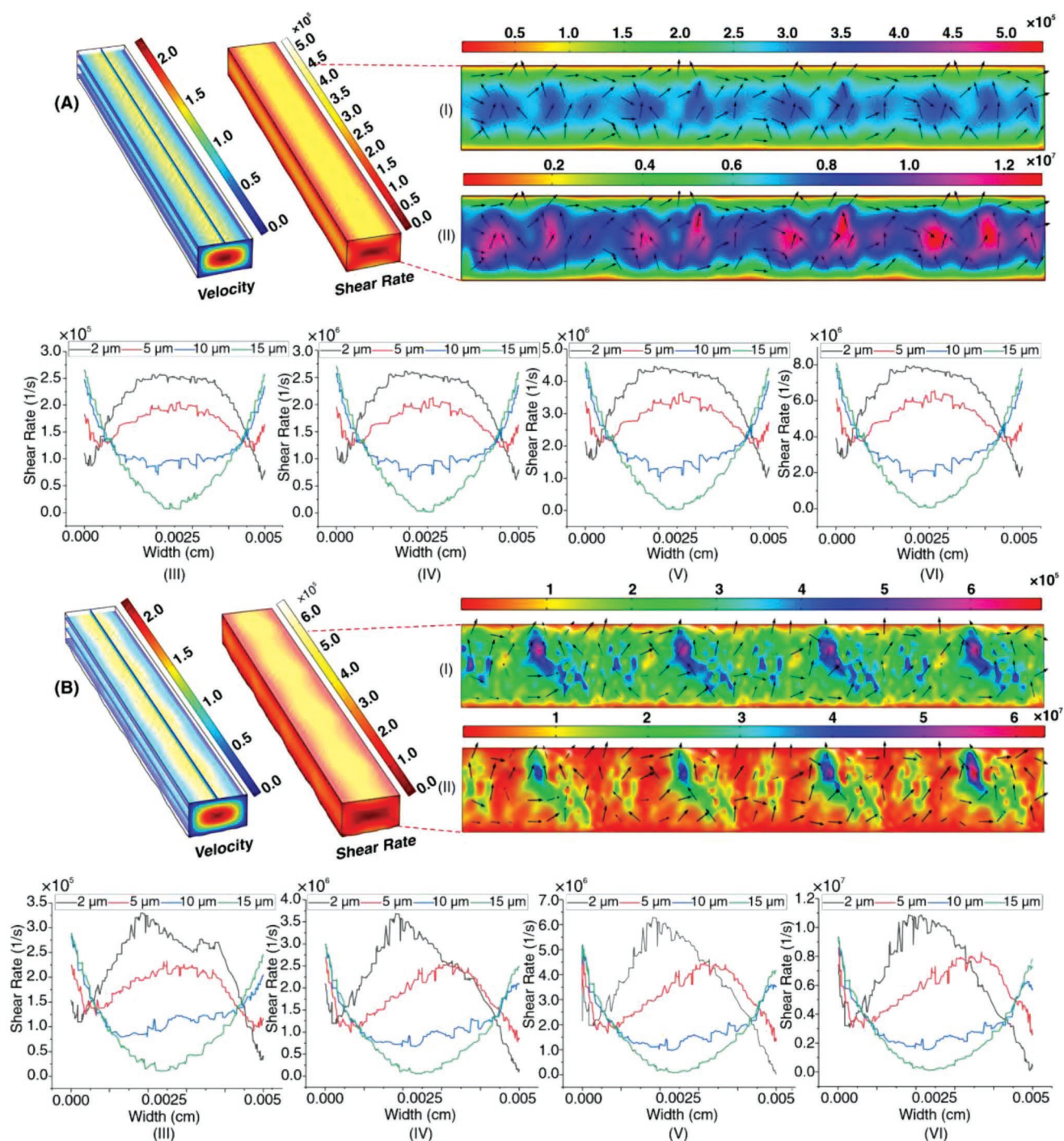


**Figure 3.** Velocity and shear rate distribution along the length of microchannel for A)  $S_a = 0.3 \mu\text{m}$  and B)  $S_a = 1 \mu\text{m}$ . Part I and II of each section (i.e., A and B) stand for the shear rate distribution at the bottom of the microchannel for velocity of 0.1 and  $3 \text{ mL min}^{-1}$  (black arrows are first principal curvature of surface). In the smooth channel, the peak of shear rate focuses at the center of the microchannel, where, in the other one, it relocates to the edges of microchannel. Shear shear distribution along the width of microchannel at 2, 5, 10, and  $15 \mu\text{m}$  for velocities of 0.1, 1, 1.7, and  $3 \text{ mL min}^{-1}$  are illustrated by parts III to VI, respectively. It shows that in rough microchannel shear rate is uneven.

of the channel. For the rough channel, although the applied flow rates were the same as the smooth channel, the shear rate distribution was noticeably greater. There is more variation in the bottom surface of the microchannel, (identified by the black arrow) when  $S_a = 1 \mu\text{m}$  compared to  $0.3 \mu\text{m}$ . The

bottom layer of the shear rate distribution also illustrates that the shear rate focuses more on the edges of the microchannel rather than in the middle (compared to the smooth surface). Thus, the probability of bonding disruption will be relocated to the edge of the channel instead of the middle of the



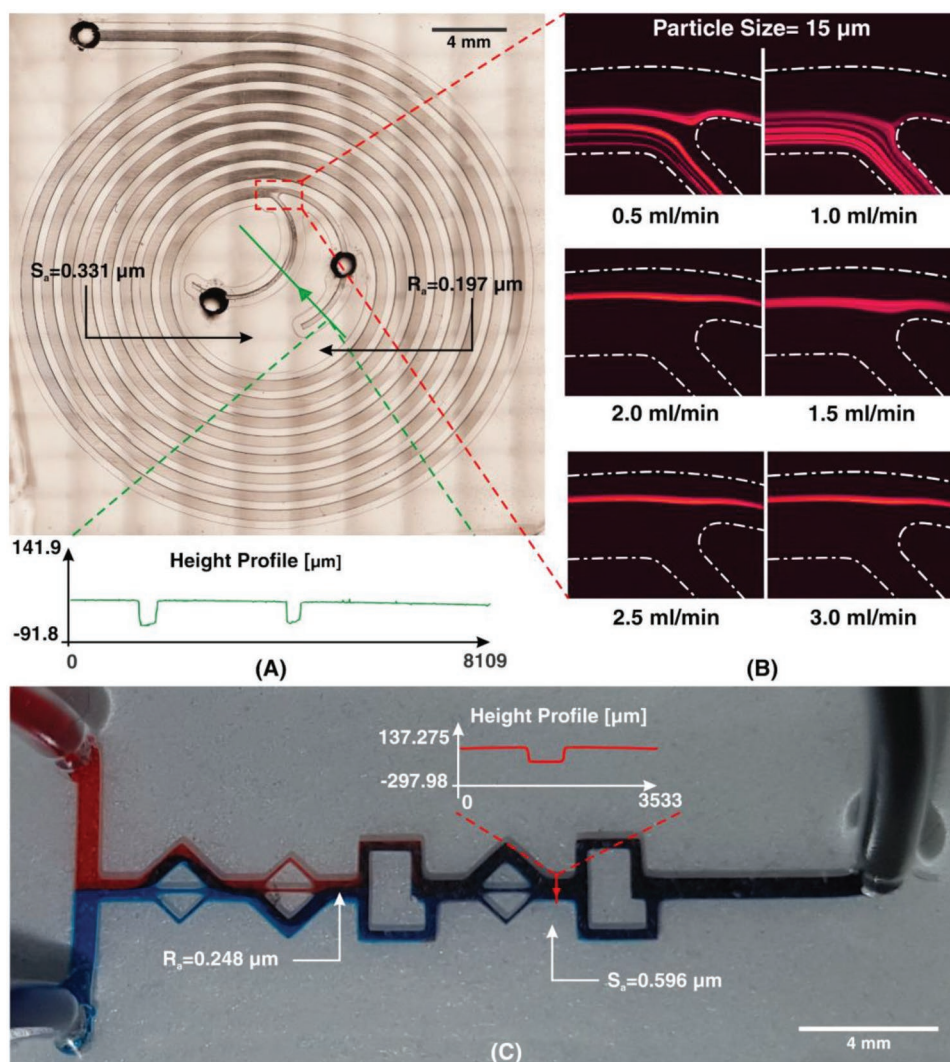


**Figure 4.** A) Whole-chip bright-field image of the spiral microchip.  $R_a$ ,  $S_a$ , and height profile are identified in the figure. B) Experimental observation of 15  $\mu\text{m}$  fluorescent beads at various flow rates from 0.5 to 3  $\text{mL min}^{-1}$ . C) Experimental observation of micromixer along the length of the microchannel with its corresponding values of  $S_a$ ,  $R_a$ , and height profile. The values of  $S_a$  reveal that PDMS microchannels from microfluidic resin are proper fluid-handling applications.

channel. Figure 3BIII–BVI show the flow rates of 0.1, 1, 1.7, and 3  $\text{mL min}^{-1}$  for  $S_a = 1 \mu\text{m}$  at a point 80  $\mu\text{m}$  after the inlet. These figures demonstrate that the shear rate distribution is uneven along the width of the microchannel. Also, the shear rate values for  $S_a = 1 \mu\text{m}$  are higher than those for  $S_a = 0.3 \mu\text{m}$  for all heights and all magnitudes of velocity. Thus, surface roughness in microfluidic devices must be small enough so as to not impact upon the performance of the device, and the bonding quality as well as measurement performed within a microchannel were not influenced by the surface roughness of the microchannel.

### 2.3. Microfluidic Devices for Liquid Handling

Particle sorting and separation have become important processes within diagnostics and biological sample handling.<sup>[30]</sup> The unique properties of fluids at the microscale can be

exploited to provide a perfect platform for handling fluid samples. For instance, fluid inertia is often used for focusing randomly dispersed particles into a particular location for the aim of collection or separation.<sup>[31,32]</sup> Spiral microchannels require relatively high flow rates which needs strong permanent bonding. In order to achieve strong bonding, the surface of PDMS layers must be ultrasmooth to facilitate plasma bonding of the PDMS and withstand the high shear stress generated by the input velocity.

Figure 4A shows the whole-chip layout of a spiral microchannel used in this study. Surface characterization depicts that the  $S_a$  is around 0.3 while  $R_a$  is approximately 0.2. As  $R_a$  is evaluated randomly in a line, it is reasonable that its value be less than that of  $S_a$  which covers the whole selected area. The function of the spiral microchip was examined with 15  $\mu\text{m}$  fluorescent particles to verify the bonding and blocking of the microchannel. Flow rates from 0.5 to 3  $\text{mL min}^{-1}$  (with an increment of 0.5  $\text{mL min}^{-1}$ ) were tested to examine the bonding

between the microchannel and its base, as shown in Figure 4B. It was illustrated that the flow behavior for these particles was the same as those reported in literature, where flow rates below  $1.5 \text{ mL min}^{-1}$  dispersed particles at the inner wall. However, at flow rates more than  $1.7 \text{ mL min}^{-1}$ , particles were focused at the outer wall and could be easily isolated for further use.<sup>[33]</sup>

Micromixers have become an essential tool in the preliminary stages of many lab-on-a-chip processes. Previously, by gaining the efficiency of proximity field nanopatterning and 3D nanolithography, Jeon et al. proposed a micromixer by implanting 3D nanostructures within the channel to enhance mixing efficiency, especially at low  $Re$  where diffusion mixing is dominant.<sup>[34]</sup> It has been proven that the combination of mixing units in micromixers improves the mixing efficiency.<sup>[35]</sup> As such, two different planar mixing units (without obstacles) were selected and connected to form a hybrid micromixer, as depicted in Figure 4C. The results of this micromixer design illustrated the efficient mixing of two fluids to give a high mixing efficiency suitable for many applications. Moreover, height profile of the channel is similar to the input CAD file. The values of  $R_a$  and  $S_a$  for this micromixer were measured to be 0.248 and 0.596, respectively. As the flow regime in microfluidic mixers usually exists at a  $Re$  of less than 100,<sup>[36]</sup> indicating laminar flow, the surface roughness does not adversely affect the function of the device.

Microfluidic devices can be integrated to act as modular components of a larger process. A decrease in the turnover time between designs as well as increased design flexibility makes 3D printing a perfect candidate for the future modularization of microfluidic devices.<sup>[37,38]</sup>

## 2.4. Biological Applications

In vitro cell culture platforms play a crucial role in cell biology, cancer research, regenerative medicine, pharmacy, and biotechnology. Although 2D cell culture in planar dishes is still widely used, this oversimplified model fails to mimic the actual cellular microenvironment. Alternatively, 3D cell culture platforms (mostly in the form of multicellular spheroids) are far more realistic models, which can better mimic in vivo responses.<sup>[39]</sup> However, these static 3D systems are still sub-optimal and lack many of the critical features essential to a complex tissue microenvironment. Additionally, these systems cannot precisely control the chemical and nutrient concentration gradients over time and space. Furthermore, the oxygen tension and shear stress experienced by the cells are different from in vivo conditions.<sup>[40]</sup> To address these shortcomings, microfluidic 2D and 3D cell culture platforms have emerged recently, progressing along with the rapid advances in microfabrication techniques.<sup>[41]</sup> Such platforms offer several advantages to engineering a physiologically relevant biomimetic tissue.

Here, we chose a pear-shaped microchamber similar to the design proposed by Chong et al.<sup>[42]</sup> The authors used the pear-shaped design to minimize the shear stress during continuous perfusion. To fabricate the arrays of the microchambers, Liu et al. used standard dry etching on a silicon substrate followed by PDMS softlithography. The dimensions and characteristics of the 3D printed microchamber are shown in Figure 5A. The total printing time starting from the initial design to the final

product took only 45 min. MCF-7 cells with a concentration of  $10^6 \text{ cells mL}^{-1}$  in culture media (Roswell Park Memorial Institute (RPMI) 1640 with 10% fetal bovine serum (FBS) and 1% streptomycin–penicillin) were introduced into PDMS microchamber. The device was incubated for 24 h at  $37^\circ\text{C}$  with 5%  $\text{CO}_2$ . To evaluate the cell viability in the PDMS microchamber, live/dead cell double staining was performed. As shown in Figure 5B,C, more than 98% of the cells remained viable in the microchamber 24 h after the initial cell seeding. This confirms that no cytotoxic residual material had been left on the PDMS from casting on the 3D printed resin. Also, in cell culture platforms, flow rates exist in the order of  $\mu\text{L min}^{-1}$ ,<sup>[43]</sup> and the values of  $R_a$  and  $S_a$ , as shown in Figure 5A, indicate that the device is functional within its flow regime. Therefore, it can be concluded that the newly developed resin for 3D printing master molds is suitable for cell culture applications and does not compromise cellular viability. Currently, lung-on-a-chip studies using 3D printed microfluidic resin molds are under investigation in our group; these studies demonstrate long-term cell viability (more than a week).

The gradient of biomolecules plays a crucial in controlling various biological activities, including cell proliferation, wound healing, and immune response. One of the most popular types of CGGs that produces discontinuous concentrations is the tree-like CGG. This type of CGG is based on the fact that one can divide and mix the flow through bifurcations and pressure differences downstream. This type of CGG is usually used for cancer cell cultures, as these CGGs transfer more oxygen and nutrients to cells as they develop a convective mass flux. Among various tree-like CGGs proposed in the literature, we chose the S-shaped CGG design developed by Hu et al.<sup>[44]</sup> The authors used micromilling to fabricate the CGG on a polymethylmethacrylate substrate. Here, we developed the same structure in PDMS using softlithography based master mold fabrication from our new microfluidic resin. Figure 4D shows the characteristics of the fabricated CGG. The device has two inlets and six outlets to produce six different concentration ranges. To examine the performance of the device, we used two colors of food dyes (please refer to the Supporting Information for dye preparation protocol). The concentration profile of the fabricated CGG is illustrated in Figure 5D, which is similar to those reported by the literature.<sup>[44]</sup> Since the velocity in CGG devices is small,<sup>[45]</sup> surface roughness cannot impose problems on the binding of PDMS. For printing of planar structures, 3D printing can be performed with higher slice thickness, as a result of which, printing time will be reduced.

In summary, the microfluidic resin for 3D printing is an ideal candidate for fabricating different bio-microfluidic devices and can replace all cost-intensive and time-consuming fabrication methods.

## 3. Conclusion

In this study, we introduced a microfluidic resin for direct fabrication of master molds for PDMS softlithography, which can substitute other time-consuming master mold fabrication methods. Conventionally, the main components of SLA/DLP

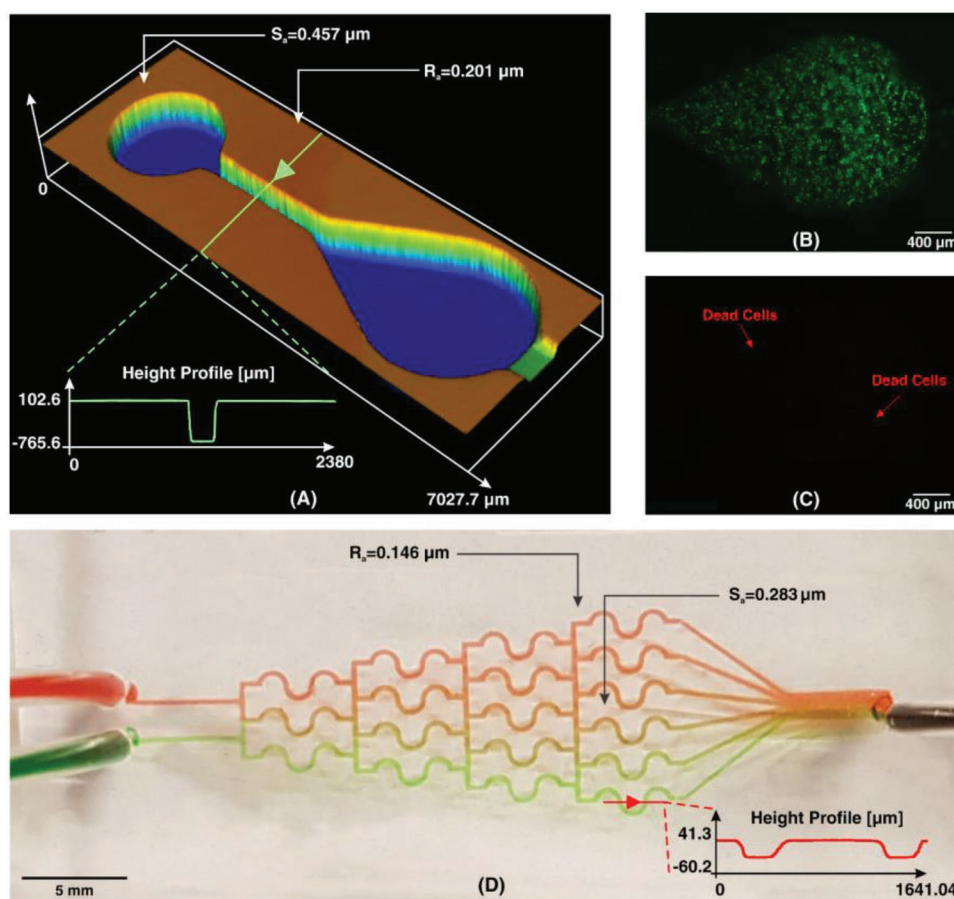


**Figure 5.** A) Whole-chip image of the cell culture device with its related  $S_a$ ,  $R_a$ , and height profile. B) Live and C) dead images of the cells after 24 h incubation, which show that cell viability in these devices are noticeable, and total numbers of dead cells are rare. D) Concentration gradient profile of two food colors of red and green. The results reveal that the newly developed microfluidic resin is suitable for cell culture applications.

resins are acrylated monomers and oligomers. These materials cannot provide a temporary attachment to PDMS without leaving uncured PDMS on the surface of the mold, indicating that the PDMS cannot replicate the mold pattern. In the proposed master mold microfluidic resin, methacrylated monomers and oligomers have been used to facilitate PDMS casting, the proof of which was illustrated by fabrication of four benchmark microfluidic devices, including separator, micromixer, cell culture device, and a concentration gradient generator. In addition, the effects of velocity and shear rate distribution on the total performance of the microfluidic device were investigated numerically. It was shown that the surface roughness has to be small enough so as to not create extra shear stress endangering PDMS bonding. As the fabricated devices were tested in wide ranges of  $Re$ , we showed that there was not any leakage in these microfluidic devices. The height profile also confirmed that there was not any major discrepancy between the CAD geometry and the fabricated part. The results of the spiral microchannel for flow rates from 0.5 to 3 mL min<sup>-1</sup> illustrated that the behavior of particles in spiral microchannel was in line with those reported in the literature, and the microchip could withstand high flow rates. The characterization of the micromixer also demonstrated that the proposed microfluidic resin was able to fabricate microchannels with different geometries,

and the mixing result was appealing so that two tested color dyes mixed completely. In the conventional softlithography process, silanization is necessary to prevent the attachment of PDMS to the master mold, which can be detrimental for cellular studies. The 3D printed mold obtained from the microfluidic resin proposed here does not require any silanization, and the cellular studies in the PDMS-based cell culture device confirmed the biocompatibility of the resin. The 3D printed CGG device produced a stable gradient profile, implying the application of such a versatile 3D printing technique for effective drug delivery. As PDMS-based microchannels are ubiquitous in microfluidic devices, the present study can be considered as a milestone in the microfluidic field which can reduce the brainstorming-to-production from a time frame of several days (including the time required for conventional master mold fabrication and post-treatment) to less than 5 h (with the new proposed microfluidic resin).

## 4. Experimental Section

**Resin:** As SLA/DLP printing process has risen in popularity, concern over its compatibility with PDMS is now an issue. The commercial resins used for DLP 3D printing of microfluidic devices were acquired from Creative CADworks company are BV-003 and BV-007 (manufactured



by MiiCraft, Taiwan), which have been broadly used in the literature<sup>[46–48]</sup> (please refer to the Supporting Information for a detailed description of these two resins). However, these resins proved to be not effective for PDMS casting. As previously mentioned, although certain surface treatments for 3D printed molds (prior to PDMS casting) have been trialed, all are either time-consuming, nonreplicable, or not effective. These two resins are composed of acrylated monomers and oligomers. However, the required surface treatment for PDMS casting impedes their further applications in microfluidic devices. Thus, methacrylated monomers and oligomers were substituted to form a microfluidic resin, which is suitable for direct PDMS casting without any post-treatment. In conventional DLP resins, COCHCH<sub>2</sub> exists in their functional groups. These components are not proper for the PDMS casting (i.e., incomplete cure of PDMS), and several groups tried to come up with a surface treatment strategy to mitigate this issue.<sup>[18]</sup> This problem is attributed to the acrylate groups, resulting in the utilization of methacrylated monomers and oligomers instead of them. Indeed, hydrogen (H) in the chemical formulation of acrylate components was replaced by methyl (CH<sub>3</sub>) to form the COCH<sub>2</sub>CH<sub>3</sub> group. The resultant resin possesses a viscosity in the range of 175–230 cps.

The polymer network of the methacrylate composites was shaped by the so-called process of “free-radical addition polymerization” of the corresponding methacrylate monomers. The process of polymerization happens in three stages, which are initiation, propagation, and termination. In this process, usually volume shrinkage is observed as a result of Van der Waals volume or the free volume reduction.<sup>[49]</sup> This volume reduction can be minimized by either adding the prepolymerized resins to the monomer resins, utilizing methacrylate monomers with high molecular mass, or increasing the percentage of inorganic filler. These monomers modify the final surface of the resin and eliminate the uncured layer in contact with the PDMS, making it appropriate for PDMS casting.<sup>[50]</sup> The exact formulations and chemical compositions of the developed microfluidic resin are proprietary to Creative CADworks.

**3D Printer Specifications, Printing Parameters, and PDMS Casting:** In this study, to create the molds, a MiiCraft Ultra 50 3D printer (MiiCraft, Hsinchu, Taiwan) was used, which has a printing area of 57 × 32 × 120 mm<sup>3</sup> and XY resolution of 30 μm. The UV wavelength used in this device is 385–405 nm, which projects from the bottom of the resin bath filled with microfluidic resin. The operating temperature is 10 to 30 °C, and the operating humidity is 40% to 60%. The desired geometries were drawn in Solidworks 2016, a commercial CAD/CAE software, and then exported with the STL file format suitable for 3D printers. The STL file is imported into the MiiCraft software (MiiCraft 125, Version 4.01, MiiCraft Inc), a software for preprocessing of design models. The imported file must be sliced to shape the desired geometry. The slicing in Z direction can be adjusted from 5 to 200 μm (with an increment of 5 μm). Reducing the thickness layer increased the final quality of the product. Since the modified resin has a high viscosity, the curing time of each layer is a challenging factor. In addition, the base and buffer layers must be carefully adjusted to allow the part to adhere to the picker without falling. When selecting a slice thickness of 10 μm for smaller features, it was better to set the curing time for each layer between 5 and 6 s. For slice thicknesses of 30 and 50 μm, the optimum curing times were found to be 6.5 and 9.5 s, respectively. The base layer is the layer that accounts for the bonding of the part to the picker. The curing time for the base layer was set to 60 s. The buffer layer was used to reduce the curing time between the base layer and subsequent part layers. As the UV light cures each layer, the Z-axis stepper motor displaced the sample one slice upward, before curing the next layer. This process continued until the whole geometry was printed. Once printed parts were removed from the picker, they were rinsed thoroughly with isopropanol. Next, an air nozzle was used to remove residual resin from the edges and in between extremely fine features. Eventually, the mold was postcured by exposing each part to the UV light in a curing chamber with a wavelength of 405 ± 5 nm. Upon fabrication of master molds, the PDMS prepolymer and the curing agent (Sylgard 184 from Dow Corning, MI, USA) were mixed in the ratio (W/W) of 10:1. This process was followed by degassing in a vacuum chamber for

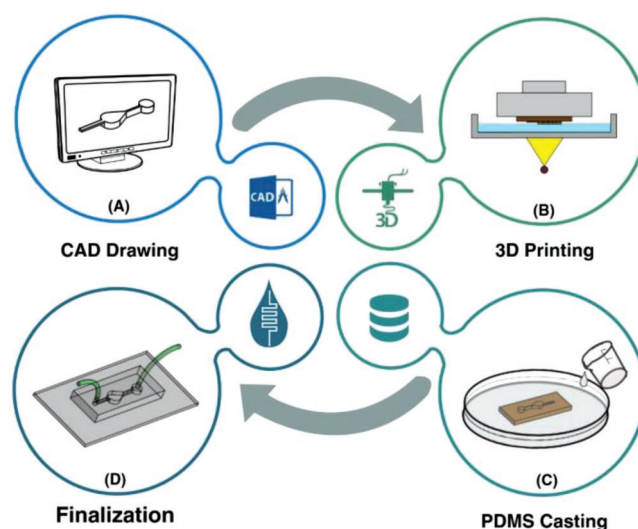


**Figure 6.** The workflow of the master mold preparation by DLP/SLA 3D printing method and microfluidic resin. A) The desired master mold is drawn. The beauty of microfluidic devices is that they require neither intricate geometries nor professional CAD drawer. Thus, the CAD drawing process will not take a long time. B) The design is then printed using a DLP/SLA 3D printer, and the residuals are removed from the surface of the mold. C) Afterward, PDMS is poured in the master mold, and D) in the final stage, PDMS is peeled-off, bonded to a glass or PDMS layer, and the finalization followed by the installation of inlets and outlets.

15 min and pouring the liquid PDMS onto the 3D printed microfluidic mold without any surface treatment process. Afterward, it was kept in an oven to complete the curing of PDMS. Subsequently, the cured PDMS was peeled off, and the inlet and outlet holes were punched. The PDMS-based microchannel was then bonded onto either a glass slide or another PDMS substrate by plasma activation to form a closed channel. The schematic illustration of microchip fabrication based on the proposed resin is illustrated in **Figure 6**.

**Benchmark Microfluidic Devices:** In order to investigate the microchips fabricated via the 3D printed microfluidic mold, four benchmark devices were tested. Generally, microfluidic devices are classified into two categories, those for liquid-handling and those for biological application.<sup>[51]</sup> To showcase liquid handling using the proposed 3D printing resin, a spiral microchip for separation and a micromixer for mixing two fluids were fabricated.

It has been shown that spiral microchannels with a trapezoidal cross-section are useful in particle/cell separation for a wide range of flow rates.<sup>[52]</sup> However, the fabrication of the mold which was mainly conducted by micromilling is a challenging process and not suitable for fabrication of complex cross-sections. By testing this device (please refer to the Supporting Information for sample preparation), the feasibility of fabricating a 3D-direct-printed spiral mold with a trapezoidal cross-section was evaluated, and the surface profile of the microchip and the bonding quality were assessed.

Mixing is an essential step in most chemical processes, and micromixer is an integral part of micro total analysis systems (μTAS). As such, the feasibility of producing planar micromixers has been showcased with a combination of two different mixing units adopted from Hossain and Kim<sup>[53]</sup> and Bhopate et al.<sup>[54]</sup> using the aforementioned technique (please refer to the Supporting Information for dye preparation). Finally, a specific design for cell culturing and concentration gradient generation for preparation of a drug with different dosages were selected. The cell culture device was selected to investigate the biocompatibility of 3D printed devices for cell culture applications (please refer to the Supporting Information for cell viability assay). The schematics of these devices with their specific dimensions are drawn in **Figure 7**.

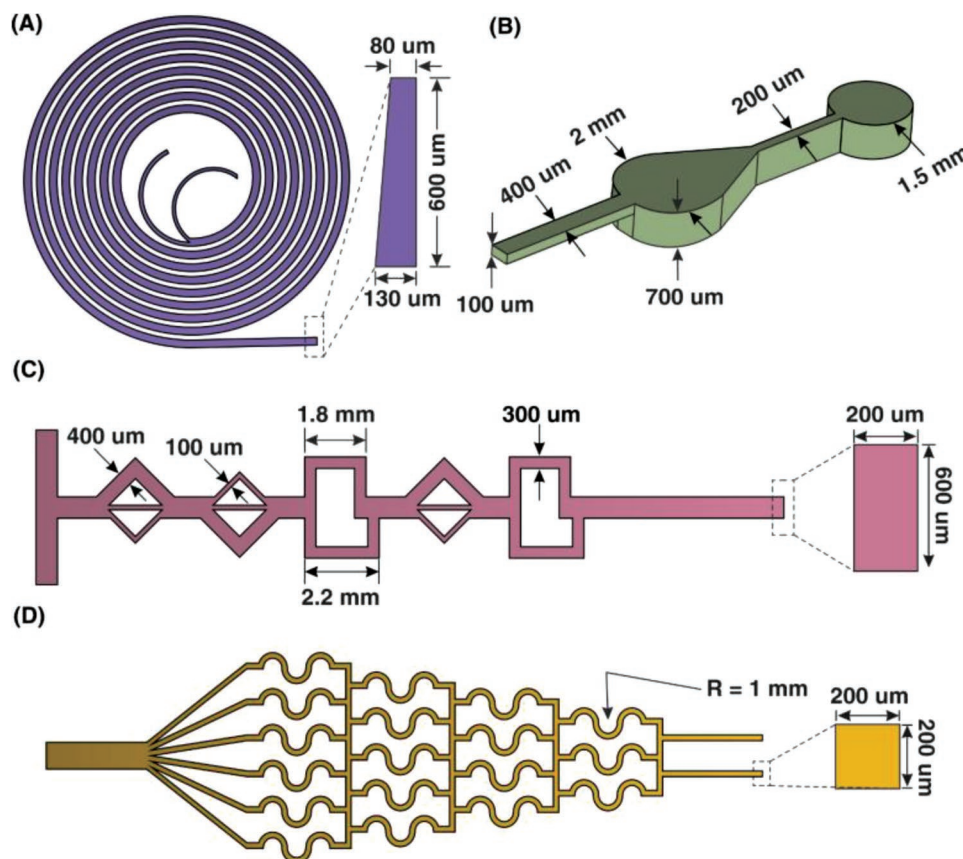


**Figure 7.** Schematic illustration of certain microfluidic devices. Generally, microfluidic devices are divided into two categories of liquid handling and biological applications. Four benchmark devices for A) particle/cell separation, B) a specific well for cell culture, C) sample mixing, and D) a concentration gradient generator with their related dimensions are selected and illustrated.

**Surface Characterization:** Surface characterizations of the 3D printed mold and PDMS were analyzed using 3D laser microscopy (Olympus LEXT OLS5000); to this end, an LMPLFLN 20× LEXT objective lens (Olympus) was selected. Arithmetic mean deviation ( $R_a$ ), the arithmetic mean of absolute ordinate  $Z(x,y)$  documented along a sampling length, and arithmetical mean height ( $S_a$ ), the arithmetic mean of the absolute ordinate  $Z(x,y)$  documented along an evaluation area were chosen to evaluate the surface characterization of the samples. In order to investigate the velocity profile and shear stress along the length of the microchannel with a rough-embedded surface, COMSOL Multiphysics 5.3a, a commercial software based on the finite element method, was used. By applying the parametric surface function within COMSOL, two different  $S_a$  values (0.3 (attributed to the measured surface roughness of the spiral microchannel) and 1  $\mu\text{m}$ ) were evaluated. To apply roughness on the bottom of the channel, Equation (1) was used

$$f(x,y) = \sum_{m=-M}^M \sum_{n=-N}^N \frac{1}{\beta} \frac{g(m,n)}{(m^2 + n^2)^{\frac{\beta}{2}}} \cos(2\pi(mx + ny) + \varphi(m,n)) \quad (1)$$

where  $x$  and  $y$  are spatial coordinates,  $N$  and  $M$  are spatial frequency resolutions. The spectral exponent is controlled by  $\beta$ , and  $g(m,n)$  and  $\varphi(m,n)$  are zero mean Gaussian and uniform (in the interval between  $-\pi/2$  and  $\pi/2$ ) random functions, respectively. In this study, the values of  $M$  and  $N$  were set to 40, and  $\beta$  was set as 2. Thereafter,  $f(x,y)$  was scaled in the  $Z$  direction to get the desired value of surface roughness.<sup>[55]</sup> Based on Equation (2), to identify the surface roughness, the amplitude parameter of  $S_a$  was used

$$S_a = \frac{1}{A} \iint_A |f(x,y)| dx dy \quad (2)$$

where the mean-plane area is identified by  $A$ . A microchannel with dimensions  $400 \times 50 \times 30 \mu\text{m}^3$  was considered, and the rough surface was applied at the bottom of the channel. In the simulations, flow was considered to be steady-state, incompressible, and Newtonian with the same properties as water. Uniform velocity was applied to the inlets, zero static pressure was assigned to the outlet, and all other walls were considered to be no-slip boundary condition.

## Supporting Information

Supporting Information is available from the Wiley Online Library or from the author.

## Acknowledgements

M.E.W. would like to acknowledge the support of the Australian Research Council through Discovery Project Grants (Grant Nos. DP170103704 and DP180103003) and the National Health and Medical Research Council through the Career Development Fellowship (Grant No. APP1143377). This work was performed in part at the South Australian node of the Australian National Fabrication Facility under the National Collaborative Research Infrastructure Strategy.

## Conflict of Interest

Kamal Patel is currently employed by Creative CADworks company. The other authors have no other relevant affiliations or financial involvement with any organization or entity with a financial interest in or financial conflict with the subject matter or materials discussed in the manuscript apart from those disclosed.

## Keywords

3D-printed molds, 3D-printing, microfluidic resin, microfluidics, soft lithography

Received: May 22, 2019

Revised: June 27, 2019

Published online:

- [1] R. Amin, S. Knowlton, A. Hart, B. Yenilmez, F. Ghaderinezhad, S. Katebifar, M. Messina, A. Khademhosseini, S. Tasoglu, *Biofabrication* **2016**, 8, 022001.
- [2] B. C. Gross, J. L. Erkal, S. Y. Lockwood, C. Chen, D. M. Spence, *Anal. Chem.* **2014**, 86, 3240.
- [3] S. Waheed, J. M. Cabot, N. P. Macdonald, T. Lewis, R. M. Guijt, B. Paull, M. C. Breadmore, *Lab Chip* **2016**, 16, 1993.
- [4] I. Wagner, Spending on 3D printing worldwide in 2019 and 2022 (in billion U.S. dollars), <https://www.statista.com/statistics/590113/worldwide-market-for-3d-printing/> (accessed: August 2018).
- [5] A. I. Shallan, P. Smejkal, M. Corban, R. M. Guijt, M. C. Breadmore, *Anal. Chem.* **2014**, 86, 3124.
- [6] C. M. B. Ho, S. H. Ng, K. H. H. Li, Y.-J. Yoon, *Lab Chip* **2015**, 15, 3627.
- [7] A. Lashkaripour, A. A. Mehrizi, M. Goharimanesh, M. Rasouli, S. R. Bazaz, *J. Mech. Med. Biol.* **2018**, 18, 1850002.
- [8] A. Lashkaripour, C. Rodriguez, L. Ortiz, D. Densmore, *Lab Chip* **2019**, 19, 1041.
- [9] M. Mollajan, S. R. Bazaz, A. A. Mehrizi, *J. Appl. Fluid Mech.* **2018**, 11, 21.
- [10] M. Rasouli, A. A. Mehrizi, M. Goharimanesh, A. Lashkaripour, S. R. Bazaz, *Chem. Eng. Process.* **2018**, 132, 175.
- [11] A. Lashkaripour, M. Goharimanesh, A. A. Mehrizi, D. Densmore, *Microelectron. J.* **2018**, 78, 73.
- [12] P. F. Costa, H. J. Albers, J. E. Linssen, H. H. Middelkamp, L. Van Der Hout, R. Passier, A. Van Den Berg, J. Malda, A. D. Van Der Meer, *Lab Chip* **2017**, 17, 2785.
- [13] T. Kwon, H. Prentice, J. De Oliveira, N. Madziva, M. E. Warkiani, J.-F. P. Hamel, J. Han, *Sci. Rep.* **2017**, 7, 6703.
- [14] J. Park, K. I. Kim, K. Kim, D. C. Kim, D. Cho, J. H. Lee, S. Jeon, *Adv. Mater.* **2015**, 27, 8000.
- [15] Z. Mahmoodi, J. Mohammadnejad, S. R. Bazaz, A. A. Mehrizi, M. A. Ghiass, M. Saidijam, R. Dinarvand, M. E. Warkiani, M. Soleimani, *Drug Delivery Transl. Res.* **2019**, 9, 707.
- [16] M. A. Raoufi, A. Mashhadian, H. Niazmand, M. Asadnia, A. Razmjou, M. E. Warkiani, *Biomicrofluidics* **2019**, 13, 034103.
- [17] N. P. Macdonald, J. M. Cabot, P. Smejkal, R. M. Guijt, B. Paull, M. C. Breadmore, *Anal. Chem.* **2017**, 89, 3858.
- [18] H. N. Chan, Y. Chen, Y. Shu, Y. Chen, Q. Tian, H. Wu, *Microfluid. Nanofluid.* **2015**, 19, 9.
- [19] T. Dinh, H.-P. Phan, N. Kashaninejad, T.-K. Nguyen, D. V. Dao, N.-T. Nguyen, *Adv. Mater. Interfaces* **2018**, 5, 1800764.
- [20] K.-i. Kamei, Y. Mashimo, Y. Koyama, C. Fockenber, M. Nakashima, M. Nakajima, J. Li, Y. Chen, *Biomed. Microdevices* **2015**, 17, 36.
- [21] G. Comina, A. Suska, D. Filippini, *Lab Chip* **2014**, 14, 424.
- [22] B. Parker, R. Samanipour, A. Ahmadi, K. Kim, *IET Micro Nano Lett.* **2016**, 11, 41.
- [23] P. H. King, G. Jones, H. Morgan, M. R. R. de Planque, K.-P. Zauner, *Lab Chip* **2014**, 14, 722.
- [24] S. Waheed, J. M. Cabot, N. P. Macdonald, U. Kalsoom, S. Farajikhah, P. C. Innis, P. N. Nesterenko, T. W. Lewis, M. C. Breadmore, B. Paull, *Sci. Rep.* **2017**, 7, 15109.
- [25] D. Karalekas, A. Aggelopoulos, *J. Mater. Process. Technol.* **2003**, 136, 146.
- [26] X. Ye, H. Liu, Y. Ding, H. Li, B. Lu, *Microelectron. Eng.* **2009**, 86, 310.
- [27] V. S. Voet, T. Strating, G. H. Schnelting, P. Dijkstra, M. Tietema, J. Xu, A. J. Woortman, K. Loos, J. Jager, R. Folkersma, *ACS Omega* **2018**, 3, 1403.
- [28] C. Charton, V. Falk, P. Marchal, F. Pla, P. Colon, *Dent. Mater.* **2007**, 23, 1447.
- [29] A. Ellakwa, N. Cho, I. B. Lee, *Dent. Mater.* **2007**, 23, 1229.
- [30] A. Tay, A. Pavesi, S. R. Yazdi, C. T. Lim, M. E. Warkiani, *Biotechnol. Adv.* **2016**, 34, 404.
- [31] A. Kulasinghe, T. H. P. Tran, T. Blick, K. O'Byrne, E. W. Thompson, M. E. Warkiani, C. Nelson, L. Kenny, C. Punyadeera, *Sci. Rep.* **2017**, 7, 42517.
- [32] M. Rafeie, J. Zhang, M. Asadnia, W. Li, M. E. Warkiani, *Lab Chip* **2016**, 16, 2791.
- [33] M. E. Warkiani, G. Guan, K. B. Luan, W. C. Lee, A. A. Bhagat, P. K. Chaudhuri, D. S. Tan, W. T. Lim, S. C. Lee, P. C. Chen, C. T. Lim, J. Han, *Lab Chip* **2014**, 14, 128.
- [34] S. Jeon, V. Malyarchuk, J. O. White, J. A. Rogers, *Nano Lett.* **2005**, 5, 1351.
- [35] S. R. Bazaz, A. A. Mehrizi, S. Ghorbani, S. Vasilescu, M. Asadnia, M. E. Warkiani, *RSC Adv.* **2018**, 8, 33103.
- [36] N.-T. Nguyen, Z. Wu, *J. Micromech. Microeng.* **2005**, 15, R1.
- [37] A. K. Au, N. Bhattacharjee, L. F. Horowitz, T. C. Chang, A. Folch, *Lab Chip* **2015**, 15, 1934.
- [38] N. Bhattacharjee, A. Urrios, S. Kang, A. Folch, *Lab Chip* **2016**, 16, 1720.
- [39] Z. Koledova, *3D Cell Culture: Methods and Protocols* **2017**, p. 1.
- [40] N. Kashaninejad, M. J. A. Shiddiky, N.-T. Nguyen, *Adv. Biosyst.* **2018**, 2, 1700197.
- [41] N. Kashaninejad, M. R. Nikmaneshi, H. Moghadas, A. Kiyomarsi Oskouei, M. Rismanian, M. Barisam, M. S. Saidi, B. Firoozabadi, *Micromachines* **2016**, 7, 130.
- [42] L. Chong, W. Lei, X. Zheng, L. Jingmin, D. Xiping, W. Qi, C. Li, *J. Micromech. Microeng.* **2012**, 22, 065008.
- [43] M. Ni, W. H. Tong, D. Choudhury, N. A. A. Rahim, C. Iliescu, H. Yu, *Int. J. Mol. Sci.* **2009**, 10, 5411.
- [44] Z. Hu, X. Chen, L. Wang, *Chem. Eng. Technol.* **2018**, 41, 489.
- [45] A. G. Toh, Z. Wang, C. Yang, N.-T. Nguyen, *Microfluid. Nanofluid.* **2014**, 16, 1.
- [46] Y.-J. Park, T. Yu, S.-J. Yim, D. You, D.-P. Kim, *Lab Chip* **2018**, 18, 1250.
- [47] E. Mattio, F. Robert-Peillard, L. Vassalo, C. Branger, A. Margailan, C. Brach-Papa, J. Knoery, J.-L. Boudenne, B. Coulomb, *Talanta* **2018**, 183, 201.
- [48] C.-K. Su, W.-C. Chen, *Microchim. Acta* **2018**, 185, 1.
- [49] J. V. Crivello, E. Reichmanis, *Chem. Mater.* **2014**, 26, 533.
- [50] R. Sakaguchi, J. Powers, *Craig's Restorative Dental Materials*, 13th ed., Mosby, Saint Louis **2012**, p.161.
- [51] N.-T. Nguyen, M. Hejazian, C. H. Ooi, N. Kashaninejad, *Micromachines* **2017**, 8, 186.
- [52] M. R. Condina, B. A. Dilmertz, S. R. Bazaz, J. Meneses, M. E. Warkiani, P. Hoffmann, *Lab Chip* **2019**, 19, 1961.
- [53] S. Hossain, K.-Y. Kim, *Micromachines* **2014**, 5, 913.
- [54] S. Bhopte, B. Sammakia, B. Murray, presented at 2010 12th IEEE Intersociety Conference on Thermal and Thermomechanical Phenomena in Electronic Systems (ITherm), Las Vegas, Nevada, USA June **2010**.
- [55] M. Villegas, Z. Cetinic, A. Shakeri, T. F. Didar, *Anal. Chim. Acta* **2018**, 1000, 248.